Single-crystal Electron Paramagnetic Resonance Investigation of γ-Irradiated $K_2[MoO(O_2)F_4]\cdot H_2O$ and Molybdenum-doped $K_2[Nb(O_2)F_5]\cdot H_2O$†

Geetha Ramakrishnan, Pillutla Sambasiva Rao and Sankaran Subramanian*
Regional Sophisticated Instrumentation Centre, Indian Institute of Technology, Madras 600 036, India

The single-crystal EPR spectra of γ-irradiated pure $K_2[MoO(O_2)F_4]\cdot H_2O$ and molybdenum-doped $K_2[Nb(O_2)F_5]\cdot H_2O$, each giving rise to a set of resonances both at low and high fields relative to that of the free-electron g value, have been investigated. The high-field lines are similar for both complexes and are attributed to an electron-excess species $[MoOF_4]^-$, formed from $[MoO(O_2)F_4]^{2-}$ by radiation damage followed by rearrangement due to the extra electron. The EPR parameters for this radical are $g_{\|} = 1.932(1)$, $g_{\perp} = 1.896(1)$, $A_{\|}(^{19}F) = 0.80(5)$ and $A_{\perp}(^{19}F) = 4.65(5)$ mT. The low-field lines of the Mo-doped niobium compound are due to a niobium hole species, $[Nb(O_2)F_5]^-$, having the unpaired electron occupying the non-bonding orbital of the peroxo oxygen atoms. However, the low-field lines of the pure molybdenum complex are due to a hole species, $[Mo(O_2)F_4]^+$, having spin-Hamiltonian parameters $g_{xx} = 2.037(1)$, $g_{yy} = 1.999(1)$, $g_{zz} = 2.011(1)$, $A_{xx}(^{19}F) = 1.81(5)$, $A_{yy}(^{19}F) = 0.70(5)$ and $A_{zz}(^{19}F) = 2.81(5)$ mT. Further support for the assumed species comes from extended Hückel molecular orbital calculations. The crystal structure of the pure molybdenum complex was redetermined.

The co-ordination chemistry of molybdenum in the oxidation states +4, +5 and +6 has received much attention due to the realization that molybdenum in these oxidation states is an essential trace element in a variety of redox enzymes.[1-20] Molybdenum is an essential micronutrient for microorganisms,[11] plants[12] and animals,[13] mainly in the form of molybdenum-bound enzymes.

Molybdenum salts are known to react with hydrogen peroxide to form a variety of complexes in which the peroxide to metal ratio varies from 1 to 4:1. The chemistry and synthesis of these complexes have been reviewed by Connor and Ebsworth.[15] A substantial number of molybdenum(VI) peroxo complexes have been structurally investigated by Weiss and co-workers[16,17] and by Stomberg and Larking.[18,19] These complexes have 'side-on' bound peroxide and are found to exist in mono-, bi-, tetra- or hepta-nuclear forms.[19] Structurally characterized peroxo compounds include $[Zn(NH_3)_4][Mo(O_2)_4]$, $[NH_4]_3[MoO(O_2)F_5]$, $K_2[MoO(O_2)F_4]\cdot H_2O$, $K_2[MoO(O_2)_2(C_2O_4)]$, $[Mo(O_2)_2\{OP(NMe_2)_3\}]\cdot H_2O$ and $[MoO(O_2)_2\{OP(NMe_2)_3\}]\cdot$py (py = pyridine). The mononuclear peroxo complexes have one Mo–O_t (O_t = terminal oxygen) bond in addition to one or two peroxo ligands. The Mo–O_t bond lengths fall in the range 1.63–1.69 Å whereas the Mo–O(peroxo) distances range from 1.91 to 1.96 Å. The peroxo ligand is always found *cis* to the oxo group, and the plane determined by the Mo–O–O ring is nearly perpendicular to the Mo–O_t direction. The peroxo complexes are of interest as reagents in organic synthesis[20] and as possible intermediates in molybdate-catalysed peroxidation and oxidation reactions.[21]

Russian workers have performed a large number of detailed EPR studies on solutions of Mo^V. In all of these studies[22-25] the complexes were not isolated, but in some cases sufficient hyperfine and superhyperfine structure was resolved to identify the stoichiometry and the structure of the species responsible for EPR absorption. Characterization of molybdenum centres, based on EPR spin-Hamiltonian parameters, has been carried out by several workers.[5,26-32]

In a previous communication[33] the EPR results obtained on γ-irradiation of $K_2[Nb(O_2)F_5]\cdot H_2O$ were discussed. Most of the spin density is on the peroxo oxygens with no superhyperfine interaction from fluorine. In continuation of this work, we undertook a study of a similar molybdenum peroxo complex, $K_2[MoO(O_2)F_4]\cdot H_2O$, to determine whether the spin density can be transferred to the fluorine ligands, and to extend the previous study by doping the niobium complex with Mo. The crystal structure of the complex has also been reinvestigated.

Experimental and Results

The vibrational and Raman spectral frequencies obtained using PE-983 IR and Cary-82 Raman spectrophotometers are consistent with the formula $K_2[MoO(O_2)F_4]\cdot H_2O$. The unit-cell dimensions and morphology were determined using an Enraf-Nonius CAD-4 four-circle X-ray diffractometer. 1545 Reflections were collected to get a better refinement of the structure than that previously obtained.[16] The details of the determination of the unit-cell parameters and structure refinement have been given elsewhere.[33]

Preparation of the Complexes.—(*a*) Dipotassium tetrafluorooxoperoxomolybdate hydrate was prepared by the method of Piccini.[34] Molybdenum trioxide (2.8 g) was dissolved in 40% HF to which 30% H_2O_2 (10 cm^3) was added. Then the stoichiometric amount of KOH solution was slowly added and the solution allowed to evaporate. The crystals were filtered from the mother-liquor and recrystallized from distilled water (Found: F, 22.4; K, 24.8; O_2^{2-}, 10.2; H_2O, 6.6. Calc.: F, 24.0; K, 24.7; O_2^{2-}, 10.1; H_2O, 5.7%).

(*b*) The salt $K_2[Nb(O_2)F_5]\cdot H_2O$ was prepared by dissolving 3 g of Nb_2O_5 (plus 5% MoO_3 as dopant) in 40% HF (10 cm^3) in a platinum crucible by heating to 475 K. The solution was cooled and filtered, and 30% H_2O_2 (10 cm^3) was added followed by a stoichiometric amount of KOH solution. The resultant solution was cooled and then allowed to evaporate slowly. The crystals obtained were washed with ethanol and diethyl ether.[35]

† *Supplementary data available* (No. SUP 56852, 3 pp.): EHMO input parameters. See Instructions for Authors, *J. Chem. Soc., Dalton Trans*, 1991, Issue 1, pp. xviii–xxii.

Non-SI unit employed: eV ≈ 1.60 × 10^{-19} J.

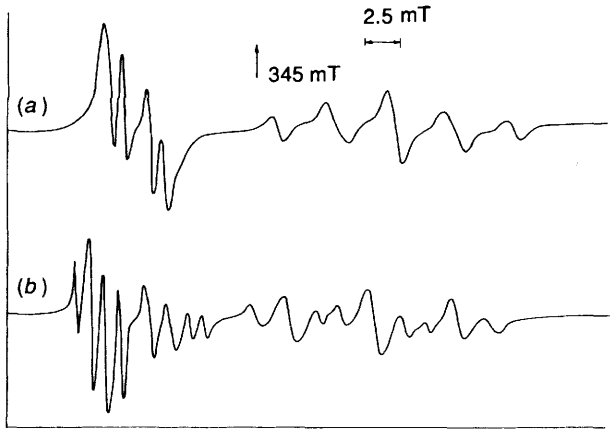

Fig. 1 Typical room-temperature X-band EPR spectra of γ-irradiated $K_2[MoO(O_2)F_4]\cdot H_2O$ crystals, indicating the low-field (<345 mT) and high-field lines (>345 mT), in the *ab* plane when the applied magnetic field is (*a*) parallel to and (*b*) 40° from the *a* axis. Frequency of measurement *ca.* 9.5 GHz for Figs. 1–6

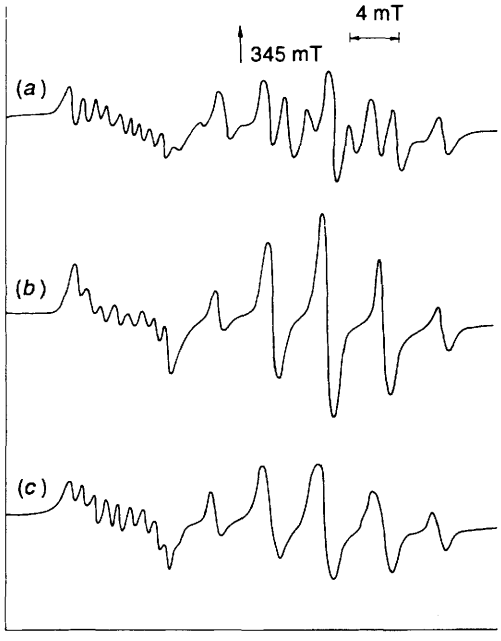

Fig. 2 Typical room-temperature X-band EPR spectra of γ-irradiated Mo-doped single crystals of $K_2[Nb(O_2)F_5]\cdot H_2O$ for rotation about the c^* axis when the applied magnetic field is (*a*) 40° from the *a* axis, (*b*) parallel to the *a* axis and (*c*) parallel to the *b* axis. Here, also, one can clearly see a set of lines both at low and high fields relative to 345 mT

Crystal Data for $K_2[MoO(O_2)F_4]\cdot H_2O$.—Monoclinic, space group $P2_1/a$, $a = 6.291(1)$, $b = 6.296(1)$, $c = 18.158(2)$ Å, $\beta = 96.9(1)°$, $Z = 4$; lit.,[16] $a = 6.308(5)$, $b = 6.274(5)$, $c = 18.166(10)$ Å, $\beta = 98.3(1)°$.

Additional data available from the Cambridge Crystallographic Data Centre comprises thermal parameters.

γ-Irradiation.—The γ-irradiation of $K_2[MoO(O_2)F_4]\cdot H_2O$ and Mo-doped $K_2[Nb(O_2)F_5]\cdot H_2O$ crystals was carried out at room temperature using a cobalt-60 source. The EPR spectra were recorded using a Varian E-112 spectrometer operating at X-band frequencies (ν *ca.* 9.5–9.9 GHz) having a 100 kHz field modulation and phase-sensitive detection to obtain the first-derivative signal. The single crystal was mounted on a Varian E-229 goniometer. The three mutually perpendicular axes *a*, *b* and c^* (c^* is perpendicular to *a* and *b*) were chosen to carry out angular variations of EPR spectra. Diphenylpicrylhydrazyl was used as an internal *g* marker ($g = 2.0036$).

Typical EPR spectra of the crystals are shown in Figs. 1 and 2, each containing sets of lines at low ($g > g_e$) and high field ($g < g_e$), where g_e is the free-electron value and corresponds to 345 mT for a frequency of 9.5 GHz. The high-field lines for the two crystals are the same but the low-field lines are different. Spectra obtained for rotation about the *a* and *b* axes are similar as regards the high-field lines for both crystals. Isofrequency plots of the high-field lines for rotation about the *a*/*b* and c^* axes are shown in Figs. 3 and 4 respectively.

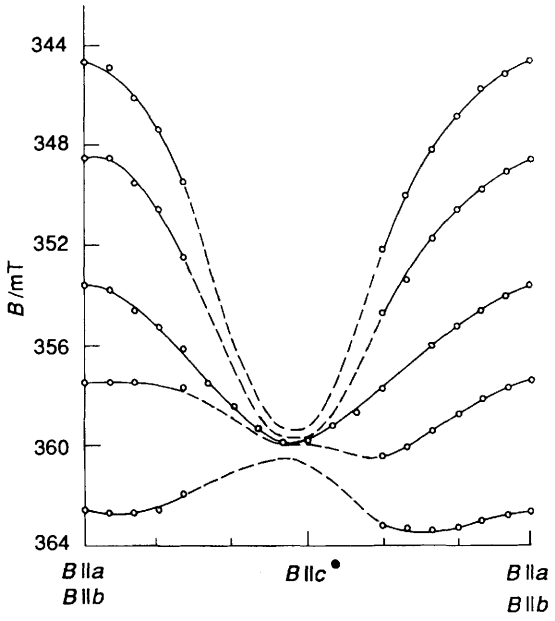

Fig. 3 Isofrequency plots of ^{19}F superhyperfine lines in the ac^* (or bc^*) plane of γ-irradiated single crystal $K_2[MoO(O_2)F_4]\cdot H_2O$ {Mo-doped $K_2[Nb(O_2)F_5]\cdot H_2O$ gives identical results} for the high-field part of the EPR spectrum at room temperature. The dashed portions indicate that the hyperfine values are within the linewidth and could not be resolved (see text)

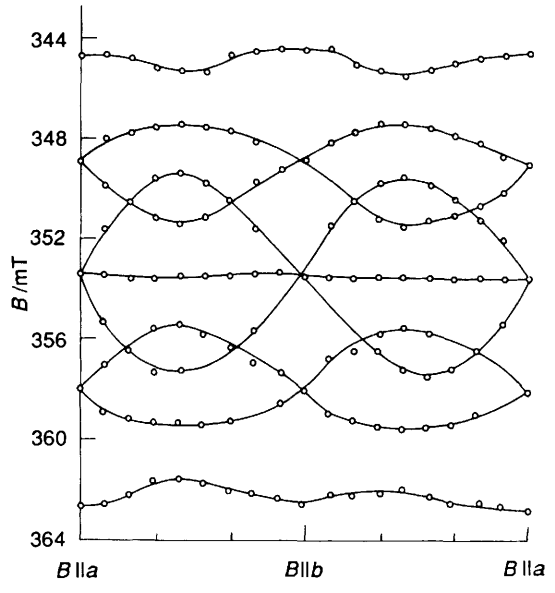

Fig. 4 Room-temperature isofrequency plot of ^{19}F superhyperfine lines in the *ab* plane for γ-irradiated single crystal $K_2[MoO(O_2)F_4]\cdot H_2O$ {Mo-doped $K_2[Nb(O_2)F_5]\cdot H_2O$ gives identical results} for the high-field part of the spectrum

The low-field lines of the Mo-doped crystal are due to a niobium hole species as discussed previously.[33] On the other hand, the low field lines of $K_2[MoO(O_2)F_4]\cdot H_2O$ are due to a Mo-centred hole species (see below). The isofrequency plots for the latter low-field lines are given in Figs. 5 and 6 respectively for two of the three mutually perpendicular planes.

Table 1 Atomic positional parameters for $K_2[MoO(O_2)F_4]\cdot H_2O$ with estimated standard deviations (e.s.d.s) in parentheses

Atom	*X/a*	*Y/b*	*Z/c*
Mo	0.2092(2)	0.1560(2)	0.1305(1)
K(1)	0.3208(5)	0.1422(5)	0.3991(2)
K(2)	0.7482(6)	0.1459(6)	0.2521(2)
F(1)	0.1785(17)	0.1691(18)	0.2408(6)
F(2)	0.4531(13)	0.3475(14)	0.1606(5)
F(3)	0.4372(14)	−0.0546(13)	0.1582(6)
F(4)	0.0583(15)	0.4310(16)	0.1263(7)
O(1)	0.2493(20)	0.1628(18)	0.0391(7)
O(2)	0.0394(19)	−0.1035(18)	0.1256(8)
O(3)	−0.0931(17)	0.0787(18)	0.1145(7)
O(W)	0.7131(21)	0.1585(19)	0.4894(7)

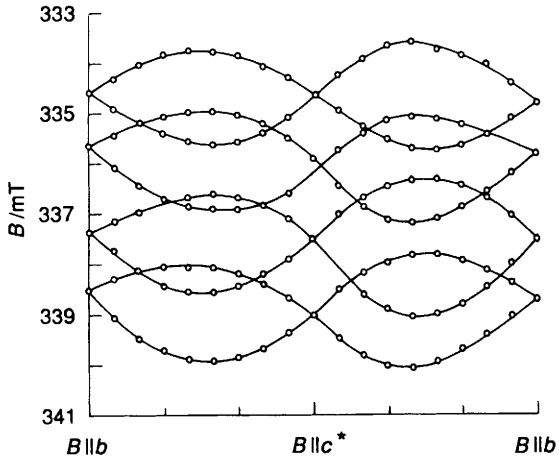

Fig. 5 Room-temperature isofrequency plot of ^{19}F superhyperfine lines in the *bc** plane of γ-irradiated single-crystal $K_2[MoO(O_2)F_4]\cdot H_2O$ for the low-field part of the spectrum

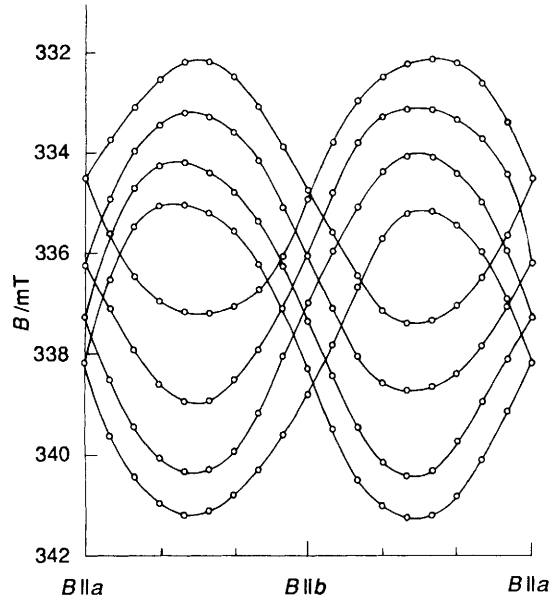

Fig. 6 Room-temperature isofrequency plot of fluorine hyperfine lines in the *ab* plane of γ-irradiated single crystal $K_2[MoO(O_2)F_4]\cdot H_2O$ for the low-field part of the spectrum

Compared to spectra at room temperature, the EPR measurements at 77 and 35 K showed an increase in intensity of the resonant lines but no change in the nature of the spectrum. Using standard procedures,[36] the *g* and *A* tensors and their direction cosines were obtained. Simulations of EPR spectra and isofrequency plots were performed with an IBM-PC/XT computer. Molecular orbital calculations were done on the molybdenum systems with the ICON-8 program[37] running on a Siemens 7580-E computer.

Table 2 Bond lengths (Å) and angles (°) in $[MnO(O_2)F_4]^{2-}$ with e.s.d.s in parentheses

Mo–F(1)	2.037(10)	Mo–O(1)	1.709(11)
Mo–F(2)	1.976(8)	Mo–O(2)	1.948(11)
Mo–F(3)	1.974(9)	Mo–O(3)	1.951(11)
Mo–F(4)	1.972(10)	O(2)–O(3)	1.419(15)
F(2)–Mo–F(1)	82.3(4)	O(2)–Mo–F(2)	158.0(5)
F(3)–Mo–F(1)	85.9(4)	O(2)–Mo–F(3)	80.0(4)
F(3)–Mo–F(2)	79.8(3)	O(2)–Mo–F(4)	118.4(4)
F(4)–Mo–F(1)	84.3(5)	O(2)–Mo–O(1)	97.0(6)
F(4)–Mo–F(2)	80.2(4)	O(3)–Mo–F(1)	87.2(5)
O(1)–Mo–F(1)	175.2(5)	O(3)–Mo–F(2)	154.7(4)
O(1)–Mo–F(2)	93.0(5)	O(3)–Mo–F(4)	75.9(4)
F(4)–Mo–F(3)	158.6(4)	O(3)–Mo–F(3)	122.4(5)
O(1)–Mo–F(3)	94.4(5)	O(3)–Mo–O(1)	96.7(6)
O(1)–Mo–F(4)	93.9(6)	O(3)–Mo–O(2)	42.7(5)
O(2)–Mo–F(1)	87.8(5)		

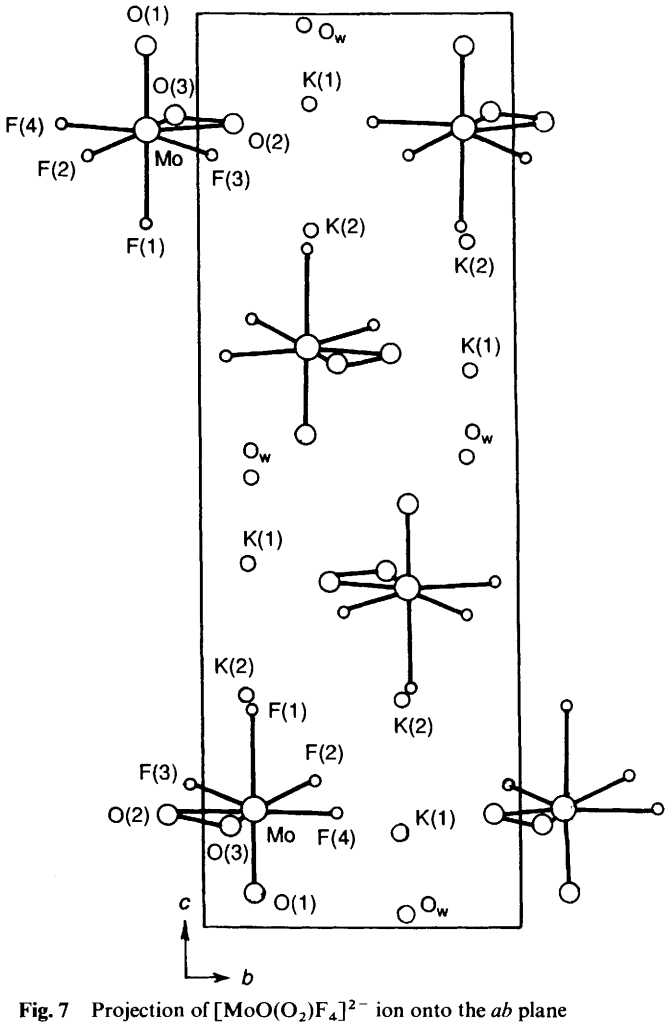

Fig. 7 Projection of $[MoO(O_2)F_4]^{2-}$ ion onto the *ab* plane

Discussion

X-Ray Data for $K_2[MoO(O_2)F_4]\cdot H_2O$.—The SHELX 86[38] program was utilized to get a rough estimate of the atomic co-ordinates after reduction of the crystal structure data. For further refinements the SHELX 76[38] program was used to give a final residual factor of 0.058, as against the previously reported value of 0.136.[16] The positional parameters, bond lengths and

Table 3 Spin-Hamiltonian parameters for some oxohalogenomolybdenum systems. The A values (in mT) are for the halide ligands

System	$g_{\parallel}$	$g_{\perp}$	$A_{\parallel}$	$A_{\perp}$	Ref.
$[MoOF_5]^{2-}$	1.911	1.874	−2.5	5.05	29
$[MoOCl_5]^{2-}$	1.963	1.940	8.15	3.60	30
	1.970	1.938	—	—	29
	1.964	1.945	0.6	—	32
$[MoOBr_5]^{2-}$	2.090	1.945	6.60	3.00	31
Powder values of Mo in different	1.943	1.950		0.20	5
ligand complexes	1.947	2.011		(^{14}N hyperfine)	
γ-Irradiated $[MoO(O_2)F_4]^{2-}$	1.932	1.896	0.8	4.65	Present work
and Mo-doped $[Nb(O_2)F_5]^{2-}$					

All g factors are correct to ±0.001 and A values to ±0.05 mT.

angles are given in Tables 1 and 2. A projection of the unit cell of $[MoO(O_2)F_4]^{2-}$ along the *bc* plane is depicted in Fig. 7. The anisotropic thermal parameters and the equations for the three least-square planes are given as the supplementary material.

In the crystal the molybdenum atom is surrounded by an oxygen [O(1)], two fluorines [F(1), F(2)] and one of the peroxo oxygen atoms [O(2)] in the equatorial plane. The apical positions are occupied by fluorines F(3) and F(4). The least-square plane analysis suggests that F(2), F(3), F(4), O(2) and O(3) also form a perfect plane indicating the presence of monocapped octahedral geometry around the metal atom. The incorporation of Mo in the lattice of $K_2[Nb(O_2)F_5]\cdot H_2O$ is evident from the similarity in geometry around the metal ions in the latter,[33] and in $K_2[MoO(O_2)F_4]\cdot H_2O$.

EPR Data.—(*a*) *γ-Irradiation of Molybdenum-doped Single crystals of* $K_2[Nb(O_2)F_5]\cdot H_2O$. Upon γ-irradiation the EPR spectra (see Fig. 2) consisted of (*i*) a niobium-centred radical with $g_{eff} > g_e$, as discussed previously,[33] and (*ii*) a molybdenum centred species with ^{19}F superhyperfine splitting having $g_{eff} < g_e$ indicating a trapped electron species. These high-field lines are similar to those found for single crystals of $K_2[MoO(O_2)F_4]\cdot H_2O$ (see below).

High-field lines. The high-field species has been identified as a molybdenum(V) d^1 system produced as a result of electron trapping by the guest complex anion $[MoO(O_2)F_4]^{2-}$ followed by loss of O_2^{2-} leading to a square-pyramidal $[MoOF_4]^-$ radical with a formal oxidation of +5 for Mo (see below). This is expected to give molybdenum hyperfine lines further split by ligand ^{19}F superhyperfine splitting. However, the satellite hyperfine lines from the relatively low abundant (25.5%) magnetic nuclei of Mo having spin $I = \frac{5}{2}$[39] are expected to be much weaker in intensity, and further reduced due to ligand (^{19}F) superhyperfine splitting. Therefore, we concentrate on the ^{19}F ligand hyperfine pattern of the molybdenum ($I = 0$) moieties and analyse it with respect to rotation of the crystal in the magnetic field. This is also the case for the complex $K_2[MoO(O_2)F_4]\cdot H_2O$.

The results of rotation about the *a* and *b* axes are similar and hence only one isofrequency plot (see Fig. 3) is shown. The five superhyperfine lines (when B is parallel to the *a* or *b* axis), due to the interaction of an electron with four equivalent ^{19}F nuclei, on rotation about the *a* or *b* axis, result in a single line (when B is parallel to the c^* axis) indicating that the hyperfine interaction is within the linewidth (≈1.0 mT) of the EPR spectrum. In other words, the contribution from the parallel component of the A tensor is minimal. Rotation about the c^* axis of the crystal results (see Fig. 4) in partial superposition of hyperfine lines. The superhyperfine interaction of the $4d^1$ electron with two non-equivalent pairs of spin $\frac{1}{2}$ (^{19}F) ligand nuclei yields a nine-line pattern (triplet of triplets) with intensity ratio 1:2:1:2:4:2:1:2:1 and fluorine hyperfine couplings of 2.0 and 6.0 mT respectively. These hyperfine lines on further crystal rotation changes into a seven-line pattern of intensity ratio 1:2:3:4:3:2:1, finally becoming five lines with the intensity distribution 1:4:6:4:1, with a fluorine hyperfine coupling constant of 4.65 mT. Based on these observations, the EPR spectra of the radical is indicative of a zero-spin nuclear species (^{94,96,98,100}Mo, 74.5% abundance), with two magnetically non-equivalent pairs of ^{19}F ligand nuclei ($I = \frac{1}{2}$), which results in a maximum of nine superhyperfine lines.

The EPR spectra correspond to an axial spin Hamiltonian[40] and the parameters obtained for the high-field lines {the results for the high-field portion of $K_2[MoO(O_2)F_4]\cdot H_2O$ are identical} are given in Table 3, along with those for a few previously reported oxohalogenomolybdenum systems. The good agreement between this radical and the other known radicals indicates that the radical is a $4d^1$ species and may be $[MoOF_4]^-$ formed from $[MoO(O_2)F_4]^{2-}$ by radiation damage followed by rearrangement (see below). The $g_{\parallel}$ value is along the *c* axis of the crystal. The observed fluorine hyperfine variation suggests four equivalent fluorines in the *ab* plane, while the crystal structure indicates only two of them in this plane. In view of this, the effect of γ-irradiation on this system requires a more detailed analysis and will be discussed in section (*c*).

(*b*) *γ-Irradiation of Single Crystals of* $K_2[MoO(O_2)F_4]\cdot H_2O$. The EPR spectra upon irradiation show signals characteristic of an electron-excess centre with $g_{eff} < g_e$, identical to that for the system discussed above. The electron-deficient species with $g_{eff} > g_e$ (low-field portion of the spectrum) is discussed below.

Low-field lines. The low-field features with $g_{eff} > g_e$ have only weak superhyperfine interaction with ligand ^{19}F nuclei. That the species is molybdenum centred has been derived from the direction cosines of the g and A tensors as well as from extended Hückel molecular orbital (EHMO) calculations (see below) which show that this species arises *via* hole trapping on a molybdenum(VI) host unit with the hole formally localized on the orbitals of ligand peroxo oxygens and that hyperfine interaction with ^{19}F arises *via* second-order spin polarization.

Rotation of the crystal about any one of the three crystallographic axis, *i.e.* *a*, *b* or c^*, resulted in a four-line pattern (doublet of doublets) when B is parallel to any one of the axes, and an eight-line pattern in other orientations. Based on the line positions and isofrequency plots (see Figs. 5 and 6), this observation can be rationalized as due to the presence of two magnetically distinct sites in the lattice with the resolved fluorine hyperfine interaction.

Based on the analysis carried out on the $K_2[Nb(O_2)F_5]\cdot H_2O$ system,[33] a single line should be observed due to the hole species created in the $K_2[MoO(O_2)F_4]\cdot H_2O$ crystal, if there is a similarity between the radical formed on γ-irradiation and the O_2^- ion. The hole species has a $g_{av} = 2.016$. The principal value of the g and A tensors are given in Table 4, along with the direction cosines of various bonds computed from single-crystal data. One of the principal values, g_{yy}, is found to lie close to the Mo–O(2) bond direction, the deviation being 12.1°. Thus, there is a possibility of spin polarization of O–Mo–F leading to ^{19}F hyperfine interaction in the hole species. The ^{19}F A tensor has one of its principal values close to the Mo–F(3) direction, the

Table 4 Spin-Hamiltonian parameters for $[MoO(O_2)F_4]^-$

	l	*m*	*n*
g_{xx} = 2.037(1)	0.720	−0.624	−0.303
g_{yy} = 1.999(1)	0.584	0.781	−0.221
g_{zz} = 2.011(1)	0.375	−0.018	0.927
$A_{xx}(^{19}F)$ = 1.81(5) mT	0.980	0.127	0.155
$A_{yy}(^{19}F)$ = 0.70(5) mT	0.308	0.818	0.431
$A_{zz}(^{19}F)$ = 2.81(5) mT	0.287	−0.338	0.896

Direction cosines (computed from crystal data) of various bonds

	l	*m*	*n*
Mo–F(1)	0.213	−0.040	−0.976
Mo–F(2)	−0.743	−0.610	−0.275
Mo–F(3)	−0.697	0.672	−0.253
Mo–F(4)	0.476	−0.878	0.038
Mo–O(1)	−0.264	−0.025	0.964
Mo–O(2)	0.543	0.839	0.045
Mo–O(3)	0.957	0.249	0.148
O(1)–O(2)	0.550	0.612	−0.569
O(2)–O(3)	0.570	−0.809	0.141
O(1)–O(3)	0.847	0.193	−0.496
Mo–½[O(2) + O(3)]	0.805	0.584	0.104

deviation being *ca.* 18°. The isotropic part of the *A* tensor is 1.77 mT, which represents a spin density of 0.1% on F. The axial fluorine interaction is negligible in the hole species formed in this system. The anisotropic components of the *A* tensors are so small in terms of actual ^{19}F p density that no useful information can be derived.

(*c*) *Radiation damage mechanism.* We now examine the possibility of radiation damage to explain the high-field lines observed in both single crystals. The primary reaction in Mo-doped $K_2[Nb(O_2)F_5]\cdot H_2O$ can lead to the formation of a $[Nb(O_2)F_5]^-$ hole species and an electron. This electron is presumably trapped on molybdenum(VI) impurity incorporated in the lattice, forming a $[MoO(O_2)F_4]^{3-}$ radical ion. The EPR spectra do not show a sharp isotropic single line at g_e, characteristic of the free electron. However, five equidistant lines with intensity ratio 1:4:6:4:1 and $g_{eff} < g_e$ suggest the formation of an electron-excess centre. The structure of the molybdenum d^1 centre produced should contain four equivalent fluorine nuclei responsible for the observed superhyperfine pattern. Considering the equivalence of ^{19}F nuclei and the crystal structure of $K_2[MoO(O_2)F_4]\cdot H_2O$, it is proposed that the $[MoO(O_2)F_4]^{3-}$ species, formed on γ-irradiation, undergoes a bond rupture at the peroxo site and transforms into a minimum-energy configuration where equivalence of the ^{19}F nuclei results. In other words, the radiation damage mechanism in equations (1)–(3) is proposed where $[MoOF_4]^-$ accounts for

$$[MoO(O_2)F_4]^{2-} \xrightarrow{h\nu} [MoO(O_2)F_4]^- + e^- \quad (1)$$

$$[MoO(O_2)F_4]^{2-} + e^- \longrightarrow [MoO(O_2)F_4]^{3-} \quad (2)$$

$$[MoO(O_2)F_4]^{3-} \longrightarrow [MoOF_4]^- + O_2^{2-} \quad (3)$$
(low *g* species)

the d^1 centre observed in both the $K_2[MoO(O_2)F_4]\cdot H_2O$ and $K_2[Nb(O_2)F_5]\cdot H_2O$ systems. When an additional electron is trapped the geometry must distort to accommodate it. As the peroxo linkage is more susceptible to bond rupture rather than are the Mo–F or Mo–O bonds, the $[MoOF_4]^-$ species is a possible product, which would account for the observed ^{19}F hyperfine splitting pattern. The similarities in the spin-Hamiltonian parameters between the present radical and other known similar radicals (Table 3) further confirms this radiation damage mechanism.

In the case of the low-field lines observed upon γ-irradiation of $K_2[MoO(O_2)F_4]\cdot H_2O$, the presence of ^{19}F hyperfine splitting indicates a rearrangement in the $[MoO(O_2)F_4]^-$ species too. The nature of the rearrangement could be as in equation (4) where we presume that an O^{2-} fragment is

$$[MoO(O_2)F_4]^- \longrightarrow [Mo(O_2)F_4]^+ + O^{2-} \quad (4)$$
(high *g* species)

eliminated leading to a $[Mo(O_2)F_4]^+$ species in which two of the fluorines are axial and two are equatorial in order to account for the observed EPR spectra. In the absence of any major rearrangement of the co-ordination polyhedron around Mo, this will lead two sets of pairs of ^{19}F nuclei. We want to emphasize here that although $[Mo(O_2)F_4]^+$ corresponds to a formal oxidation of +7 for molybdenum, the 'hole' is entirely confined to the non-bonding orbital of the peroxo oxygen (see below). Therefore, the species is similar to $[NbO_4]^{2-}$ (formal oxidation state +6) produced by hole trapping on $[NbO_4]^{3-}$-doped $CaWO_4$,[41,42] for which the metal hyperfine coupling constant was found to be *ca.* 20 G. In such hole species the metal hyperfine coupling which arises *via* configuration interaction leads to less than 0.5% spin density. In our case, this small amount of transferred unpaired spin density on molybdenum is subjected to hyperfine interaction from the 25% abundant magnetic nuclei of Mo ($I = \frac{5}{2}$) and further by four ^{19}F nuclei leading to satellite hyperfine structure of negligible intensity. The spectra from Mo ($I = 0$) with superhyperfine coupling to two inequivalent ^{19}F ligands are the ones we are considering here. The above mechanisms are qualitatively supported by EHMO calculations done on the assumed species and the results are given below.

EHMO Calculations.—The EHMO calculations were done on $[MoO(O_2)F_4]^{2-}$ using the parameters (Slater orbital exponents and valence state ionization energies) given in ref. 43. The resultant energy-level diagram is shown in Fig. 8. The possibility of an electron-excess centre as well as a hole species formation can be rationalized based on the MO scheme. From the EHMO calculations, the highest occupied molecular orbital (HOMO) (ascertained to be the non-bonding orbital of the peroxo oxygen atoms) is found to be $\psi_{HOMO} = 0.1103\ p_x$ [O(2)] − 0.0498 p_y [O(2)] − 0.7272 p_z [O(2)] − 0.1095 p_x [O(3)] + 0.0497 p_y [O(3)] + 0.7279 p_z [O(3)]. This clearly indicates that the electron removed during γ-irradiation has come from the oxygen atoms of the peroxo group and not from the central metal atom. Further, EHMO calculations done on the $[MoOF_4]^-$ radical and $[Mo(O_2)F_4]^+$ hole species also indicate good agreement with our experimental observation. Thus, the γ-irradiation of the molybdenum complex results in an electron-excess centre and a hole species whose possible structures have been deduced from their respective EPR spectra.

Conclusion

The molybdenum-doped $K_2[(Nb(O_2)F_5]\cdot H_2O$ and $K_2[MoO(O_2)F_4]\cdot H_2O$ systems behave similarly on γ-irradiation producing a $4d^1$ molybdenum(V) centre. The EPR spectral features have been analysed based on the axial spin-Hamiltonian parameters. The structure of the centre has been deduced and a plausible radiation damage mechanism proposed. In addition to the d^1 molybdenum centre, a hole species is also formed, as discussed previously[33] for the niobium system, and that $K_2[MoO(O_2)F_4]\cdot H_2O$ behaves differently. The salient features of the hole species are the hyperfine coupling to only two of the four ^{19}F ligands and the presence of two different sites in the $K_2[MoO(O_2)F_4]\cdot H_2O$ system. Thus, EPR has proven useful in identifying the paramagnetic centres and also yielding information about their location, orientation

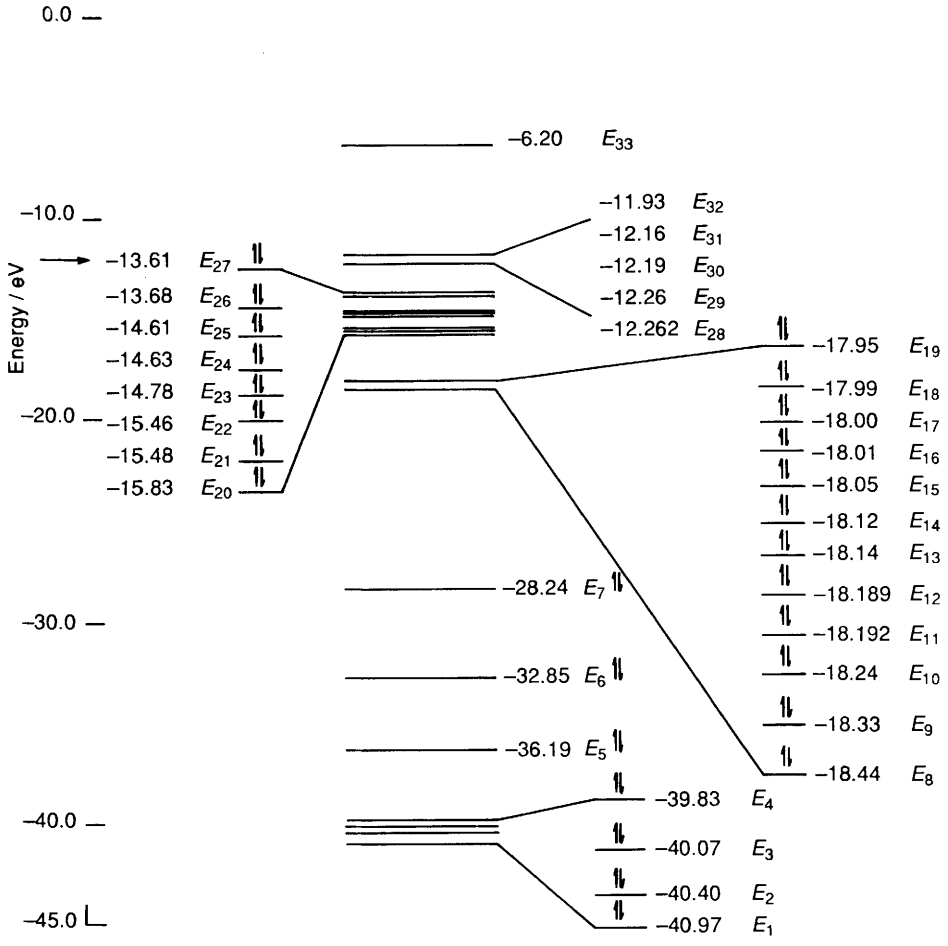

Fig. 8 Energy-level diagram of $[MoO(O_2)F_4]^{2-}$ ion, obtained from EHMO calculations. The arrow (⟶) indicates the highest occupied molecular orbital, coefficients for which are given in the text

and structure. Although no metal hyperfine is observed for these two centres, the directions of the *g* and ligand-hyperfine tensors clearly indicate that the radicals responsible for the observed spectra arise from metal-centred species and are not due to radicals exclusively having fluorine and/or oxygen atoms only.

Acknowledgements

G. R. thanks the Indian Institute of Technology, Madras, for allowing her to pursue research on a part-time basis and P. S. R. thanks the Council of Scientific and Industrial Research, India for a fellowship. Thanks are also due to Dr. Babu Varghese for his help in the crystal structure determination of the molybdenum complex.

References

1 R. C. Bray, *Adv. Enzymol, Relat. Areas Mol. Biol.*, 1980, **51**, 107.
2 E. J. Hewitt and B. A. Notton, *Molybdenum and Molybdenum containing Enzymes*, ed. M. Coughlan, Pergamon, New York, 1980, p. 273.
3 D. H. Killeffer and A. Linz, *Molybdenum Compounds, their Chemistry and Technology*, Interscience, New York, 1952.
4 F. A. Cotton, M. P. Diebold, C. J. O'Connor and G. L. Powell, *J. Am. Chem. Soc.*, 1985, **107**, 7438.
5 P. Subramanian, J. T. Spence, R. Ortega and J. H. Enemark, *Inorg. Chem.*, 1984, **23**, 2564 and refs. therein.
6 P. C. H. Mitchell, *Coord. Chem. Rev.*, 1966, **1**, 315; *Q. Rev. Chem. Soc.*, 1966, 103.
7 J. T. Spence, *Metal ions in Biological Systems*, vol. 5, ed. H. Sigel, Marcel Dekker, New York, 1979; *Coord. Chem. Rev.*, 1969, **4**, 475.
8 F. L. Bowden, *Techniques and Topics in Bioinorganic Chemistry*, ed. C. A. McAuliffe, Halstead Press, Wiley, New York, 1975, p. 205.
9 B. Spirack and Z. Dori, *Coord. Chem. Rev.*, 1975, **17**, 99.
10 F. A. Schroeder, *Acta Crystallogr., Sect. B*, 1975, **31**, 2294.
11 J. Levy, J. J. R. Campbell and T. H. Blackburn, *Introductory Microbiology*, Wiley, New York, 1973.
12 E. J. Hewitt, *Biol. Rev.*, 1959, **34**, 333.
13 E. J. Underwood, *Trace Elements in Human and Animal Nutrition*, 3rd edn., Academic Press, New York, 1971.
14 E. I. Stiefel, *Prog. Inorg. Chem.*, 1977, **22**, 1.
15 J. A. Connor and E. J. Ebsworth, *Adv. Inorg. Chem. Radiochem.*, 1964, **6**, 280.
16 D. Grandjean and R. Weiss, *Bull. Soc. Chim. Fr.*, 1967, **34**, 3044.
17 L. M. LeCarpentier, A. Mitschler and R. Weiss, *Acta Crystallogr., Sect. B*, 1972, **28**, 1278, 1288; *Chem. Commun.*, 1968, 1260.
18 I. Larking and R. Stomberg, *Acta Chem. Scand.*, 1970, **24**, 2034.
19 R. Stomberg, *Acta Chem. Scand.*, 1970, **24**, 2024; 1968, **22**, 1076.
20 N. A. Johnson and E. S. Gould, *Inorg. Chem.*, 1967, **39**, 407.
21 C. C. Su, J. W. Reed and E. S. Gould, *Inorg. Chem.*, 1967, **12**, 337.
22 N. S. Garif'yanov, V. N. Fedotov and N. S. Kuchenyavnko, *Izv. Akad. Nauk SSSR, Ser. Khim.*, 1964, 743.
23 N. S. Garif'yanov and S. E. Kamenev, *Russ. J. Phys. Chem.*, 1969, **43**, 609.
24 I. N. Marov, V. K. Belyaeva, Y. K. Dubrov and A. N. Ermakov, *Dokl. Akad. Nauk SSSR*, 1967, **177**, 1166; *Russ. J. Inorg. Chem.*, 1972, **17**, 515.
25 G. M. Larin, P. M. Solozhenkin and E. V. Semenov, *Dokl. Akad. Nauk SSSR, Ser. Khim.*, 1974, **214**, 1343.
26 R. C. Bray and L. S. Meriwether, *Nature (London)*, 1966, **212**, 467.
27 T. Hwang and G. P. Haight, jun., *J. Am. Chem. Soc.*, 1970, **92**, 2336; 1971, **93**, 611.
28 P. C. H. Mitchell and R. D. Searle, *Proceedings of the First International Conference on Chemistry and Uses of Molybdenum*, ed. P. C. H. Mitchell, Climax Molybdenum Co., 1974.
29 P. T. Manoharan and M. T. Rogers, *J. Chem. Phys.*, 1968, **49**, 5510.
30 H. Kon and N. E. Sharpless, *J. Phys. Chem.*, 1966, **70**, 105.

31 K. DeArmond, B. B. Garrett and H. S. Gutowsky, *J. Chem. Phys.*, 1965, **42**, 1019.
32 S. Radhakrishna, B. V. R. Chowdari and A. K. Viswanath, *J. Chem. Phys.*, 1977, **66**, 1019.
33 R. Geetha, P. Sambasiva Rao, B. Varghese and S. Subramanian, *Inorg. Chem.*, 1991, **30**, 1630.
34 A. Piccini, *Z. Anorg. Chem.*, 1892, **1**, 52.
35 N. Vuletic and C. Djordjevic, *J. Less-Common Met.*, 1976, **45**, 85.
36 D. S. Schonland, *Proc. Phys. Soc.*, 1959, **73**, 788.
37 ICON 8: J. Howell, A. Rossi, D. Wallace, K. Haraki and R. Hoffman, *Quantum Chemical Program Exchange*, 1977, **11**, 344.
38 G. M. Sheldrick, SHELX 76, Program for Crystal Structure Determination, University of Cambridge, 1976; SHELX 86, University of Göttingen, 1986.
39 P. S. Rao and J. A. Weil, *Nuclear (Ground State) Properties useful for EPR Spectroscopists*, Bruker Analytische Messtechnik, Rheinstetten, 1983.
40 A. Abragam and B. Bleaney, *Electron Paramagnetic Resonance of Transition Ions*, Clarendon Press, Oxford, 1970.
41 P. R. Edwards, S. Subramanian and M. C. R. Symons, *J. Chem. Soc. A*, 1968, 2985.
42 K. C. Chu, C. Kikuchi and W. Viehmann, *J. Chem. Phys.*, 1967, **46**, 386.
43 M. H. Whangbo and F. Foscher, *Inorg. Chem.*, 1981, **20**, 113.

Received 25*th March* 1991; *Paper* 1/01411K